Constraints on Scalar Millicharged Particles from Hydrogen Spectroscopy

Logan Gates
Supervisor: Dr. Alexander Penin

December 2, 2019

Abstract

The objective of this paper was to further constrain scalar Millicharged particles charge-mass phase space. The Millicharge's contribution to the Lamb Shift (for the $2S_{\frac{1}{2}}$ and $2P_{\frac{1}{2}}$ splitting) was computed by analyzing the 1-loop corrections to the Coulomb potential, allowing for the energy splitting to be determined. Comparing to the current restrictions on the charge and mass, this analysis, for $m > m_e$, does not alter the constraints. However, for $\frac{m}{m_e} \leq 7.297 \times 10^{-4}$, the current limit of $\epsilon < 1 \times 10^{-5}$ has been constrained to $\epsilon < 3.011 \times 10^{-6}$.

Contents

Introduction

2012 marked a significant achievement for particle physics with the discovery of the Higgs Boson since all the constituents, predicted by the Standard Model, were discovered. Albeit a historic moment for the field, the Standard Model fails to explain phenomena, such as dark matter, dark energy, and Quantum Gravity. Consequently, theorists attempt to create Beyond the Standard Model theories to explain such phenomenon, while experimentalists try to verify or disregard the proposed theories. Even with experiments probing higher and higher energy scales, as of now, there as been iota success. As the energy scales increase, the difficulty in reaching them does too, which results in an increased difficulty in probing some theories.

Millicharged particles (MCP), a potential solution to the demand for higher energy experiments, were first proposed, seemingly, by [4] in 1979 and [8] in 1986, and they remain of interest to this day. MCP are a hypothesized particle with a small mass, m, and a charge, $q_M = \epsilon e$, much less than the elementary charge, e, where $\epsilon << 1$- hence the name "millicharged." Their small charge results in them weakly interacting with ordinary matter, meaning MCP would have evaded detection at lower energy scales [15]. Instead of searching for new physics at high energy, high precision tests at lower energies could potentially lead to the discovery of the MCP, especially considering dark matter challenges the notion new physics is only at the high energy frontier [5]. Typically, MCP are studied as a scalar or fermion [3]; in this paper, they will be analyzed as the scalar variety.

MCP have become important in physics, specifically as a potential solution to dark matter, as they appear naturally in many theories [3]. Typically, they are introduced by implementing a new (hidden sector) gauge group, $U_{HS}(1)$, with a corresponding gauge field, A'_μ, called the dark photon. Under the assumption the dark photon field is massless, MCP appear. Albeit there is no guarantee dark matter will interact with ordinary matter, kinetic mixing serves as a possible avenue for it to interact; with a kinetic mixing term $\frac{\epsilon}{2}F'_{\mu\nu}F^{\mu\nu}$ between dark photons and photons, ordinary matter does not obtain extra charge, while MCP do acquire a small charge with respect to "our world," leading to potential interactions from it with ordinary matter [3, 11, 16].

Albeit important to dark matter, MCP also appear in other areas of physics as a potential solution, such as to the strong-CP problem [7], they could impact Big Bang Nucleosynthesis by increasing ^4He production [25] and/or influencing the baryon-to-photon ratio [24], and they might impact the luminosity distance from supernova surveys, resulting in dimming [17]. The expansion rate of Universe, the creation of galactic magnetic fields during galaxy formation, and the anisotropy power spectrum of the Cosmic Microwave Background could be affected [24]. To test for their existence, there are a multitude of methods; here is a general, non-complete list. They could be detected by light shining through a wall experiment [6], proton and electron beam dump experiments [12], or in dark photon production and decay at the NA64 experiment at CERN [23]. Proton fixed target experiments have also been proposed [3]. MCP might also be produced at nuclear reactors, be a product of gamma rays interacting with the atmosphere, or dark matter gamma rays, consisting of MCP, may accompany ordinary gamma rays, bombarding earth's atmosphere [16]. Certain rare positronium decays, resulting in invisible final states, could be an indicator of MCP [2], or liquid argon neutrino experiments might detect them [18]. SLAC has, as well, been utilized to search for MCP [1]. The Cosmic Microwave Background and Big Bang Nucleosynthesis have been used to put constraints on the MCP [16] and could indicate they exist [11]; if Cosmic Microwave Background photons are lost due to MCP pair production in galaxy cluster's magnetic fields, anisotropies could provide information on the MCP's properties [9].

So far, from the experiments and searches, the charge-mass phase space of the MCP has been constrained. Let $m = \mu m_e$, resulting in 1keV $\mapsto \mu = 1.957 \times 10^{-3}$. For $\mu < 1$, the constraints are much stronger. Reactor experiments have placed a strict limit of $\epsilon < 1 \times 10^{-5}$ for $\mu < 1.957 \times 10^{-3}$ [3, 24]; for $\mu < 1$ but $\mu > 1.957 \times 10^{-3}$, ortho-positronium decays provide the limit of $\epsilon < 3.4 \times 10^{-5}$ [2]. For $\mu > 1$, the bounds are weaker with the following: for $\mu = 1.957$, $\epsilon < 4.1 \times 10^{-5}$ and, for $\mu = 1.957 \times 10^2$, $\epsilon < 5.8 \times 10^{-4}$ [1]; for $\mu > 1.957 \times 10^2$, $\epsilon \sim 10^{-2}$ and, for $\mu > 1.957 \times 10^3$, a maximum restraint is reached at $\epsilon = 0.1$ [3, 24], implying there is an overall constraint of $\epsilon \leq 0.1 \, \forall \mu$.

Albeit there are a lot of ways to probe for MCP, we, in this paper, will be looking at Hydrogen Spectroscopy- specifically, the Lamb Shift, the energy level difference between $2S_{\frac{1}{2}}$ and $2P_{\frac{1}{2}}$ in hydrogen, which is caused by vacuum polarization- as a method to search for them. Since MCP weakly interact with matter, and there already exists heavy constraints on them, one will require high precision testing to detect them. Since hydrogen energy level transitions undergo high precision testing and are some of the best studied observables [14, 21], and the Lamb Shift is one of the most precise measurements made [20], it is an obvious avenue to probe for MCP.

To accomplish this, the scattering of two fermions, coupled to the Electromagnetic field, will be analyzed in the non-relativistic limit. The 1-loop corrections will be examined; instead of a fermion-antifermion loop, the loop will consist of MCP, coupled to the Electromagnetic field. Since the Electromagnetic field is a gauge theory, where its Lagrangian is given by: $\mathcal{L}_{EM} = -\frac{1}{4} F_{\mu\nu} F^{\mu\nu}$, the MCP field must be a gauge theory as well, thereby forcing it to be a complex scalar field so that it is invariant under the global $U(1)$ transformation. The massive complex scalar field Lagrangian [13, 22] will be used, which is given by:

$$\mathcal{L}_{MCP} = \partial^\mu \psi^\dagger \partial_\mu \psi - m^2 \psi^\dagger \psi$$

To make the MCP a gauge theory- namely, invariant under a local $U(1)$ transformation- the gauge field, A_μ, is introduced and the minimal coupling prescription (i.e. $\partial_\mu \mapsto D_\mu = \partial_\mu + i q_M A_\mu$) is followed [22]. Following this, we obtain the interaction Lagrangian for the MCP:

$$\mathcal{L}_{int} = i q_M \left[(\partial^\mu \psi^\dagger) A_\mu \psi - A^\mu \psi^\dagger (\partial_\mu \psi) \right] + q_M^2 \psi^\dagger \psi A^\mu A_\mu$$

from this, the Feynman rules were derived and can be found in Appendix A.

The scattering amplitude of the fermions, interacting with the corrected photon propagator, will be calculated. Since we are considering the hydrogen atom, a bound state problem, the fermions will be a proton and an electron. Using the Born-Approximation of the differential cross-section, a relation between the Coulomb potential and the scattering amplitude will be established, which will give the corrected Coulomb potential. Since the MCP mass is not known, the mass limits will be taken- namely, it will be assumed $m^2 << \vec{p}^2$, the low mass limit, and $m^2 >> \vec{p}^2$, the high mass limit, where $\vec{p}$ is the 3-momentum of the photon.

An experimental value, allowing the prediction to be verified, will be calculated. The contribution to the Lamb Shift due to the MCP 1-loop diagrams will be computed from $\Delta E = \langle\psi|\Delta V|\psi\rangle$, where ΔE is the energy splitting of the hydrogen atom, ψ is the hydrogen atom's wavefunction, and ΔV is the correction term due to the MCP in the corrected Coulomb potential. Since q_M and m are not known, and ΔE will depend on those parameters, we will plot q_M versus m for a corresponding energy, which will give bounds on both q_M and m.

Natural units ($c = \hbar = 1$) and Heaviside-Lorentz units ($\epsilon_o = \mu_o = 1$) will be used.

Corrected Coulomb Potential

For fermion-fermion scattering with 1-loop MCP corrections, the relevant Feynman diagrams are:

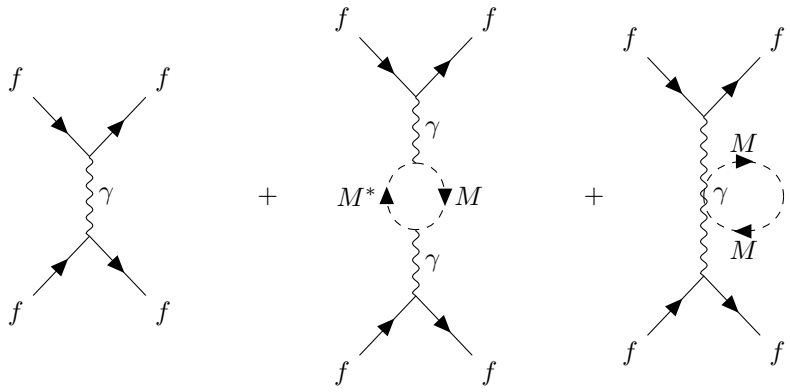

The photon propagator will be redefined to include all of its self-energy (i.e. the sum of all 1-part irreducible (1PI) diagrams), $i\Pi_2^{\mu\nu}$. It becomes: $D_{\mu\nu} = D^o_{\mu\nu} + D^o_{\mu\lambda} i\Pi^{\lambda\eta} D^o_{\eta\nu} + ...$, where $D^o_{\mu\nu} = \frac{-ig_{\mu\nu}}{p^2+i\epsilon'}$ [22]. For 1-loop corrections to second order, $D_{\mu\nu} = D^o_{\mu\nu} + D^o_{\mu\lambda} i\Pi_2^{\lambda\eta} D^o_{\eta\nu}$, where:

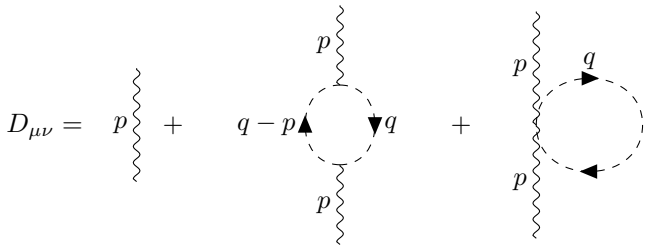

where p is the photons and q is the MCP's 4-momentum. The 1PI self-energy will be calculated by evaluating the two 1-loop diagrams for the MCP. Writing down and summing the amplitudes for the diagrams:

$$i\Pi_2^{\mu\nu} = q_M^2 \int \frac{(2q^\mu - p^\mu)(2q^\nu - p^\nu) - 2g^{\mu\nu}\left((q-p)^2 - m^2\right)}{((q-p)^2 - m^2 + i\epsilon')(q^2 - m^2 + i\epsilon')} \frac{d^4q}{(2\pi)^4}$$

The full calculation can be found in Appendix C. After evaluating it, one obtains:

$$i\Pi_2^{\mu\nu} = -iq_M^2 p^2 g^{\mu\nu} \Pi_2(p)$$

where $\Pi_2(p) = \frac{1}{8\pi^2} \int_0^1 x(2x-1)\left[\frac{2}{\epsilon'} + \ln\left(\frac{4\pi e^{-\gamma_e}\mu^2}{p^2 x(x-1)+m^2}\right) + \mathcal{O}(\epsilon')\right] dx$ and γ_e is the Euler-Mascheroni constant. A relationship between the corrected Coulomb potential and the scattering amplitude will be established in Appendix C. The corrected Coulomb potential obtained is:

$$\tilde{V}(p) = \frac{q_f^2}{p^2}\left[1 - q_M^2 \Pi_2(p)\right]$$

To renormalize it, we will use the on-shell renormalization condition. In classical Electrodynamics, we know: $\tilde{V}(p_o) = \frac{e^2}{p_o^2}$, where e is the experimentally measured charge of the electron and proton, and p_o is the momentum one made the measurement at. As $p \mapsto 0$, we should obtain the macroscopically measured charge value of e. Setting $p_o = 0$ and requiring our expression match experiment, we get: $e^2 = p_o^2 \tilde{V}(p_o) = q_f^2\left[1 - q_M^2\Pi_2(p_o)\right] \implies e^2 = q_f^2\left[1 - q_M^2\Pi_2(0)\right] \implies$ we want: $\Pi_2(0) = 0 \implies$ introducing a counterterm: $\Pi_2(p) \mapsto \Pi_2(p) - \Pi_2(0)$. With the pole removed, we have obtained the renormalized Coulomb potential, where we have replaced q_f, the bare charge, with e, the renormalized charge:

$$\tilde{V}(p) = \frac{e^2}{p^2}\left[1 - q_M^2 \Pi_2^R(p)\right]$$

where $\Pi_2^R(p) = \Pi_2(p) - \Pi_2(0) = \frac{1}{8\pi^2} \int_0^1 x(2x-1) \ln\left[\frac{m^2}{m^2 + p^2 x(x-1)}\right] dx$. The evaluation of the mass limits can be found in Appendix D; the calculation of ΔE can be found in Appendix E. The results are summarized in Table 1.

Table 1: Mass Limits of the Corrected Coulomb Potential and the Corresponding Energy Splitting

Small Mass Limit ($m^2 << \vec{p}^2$)	Large Mass Limit ($m^2 >> \vec{p}^2$)
$\tilde{V}(\vec{p}) = -\frac{e^2}{\vec{p}^2}\left[1 + \frac{q_M^2}{48\pi^2}\ln\left(\frac{\vec{p}^2}{m^2}\right)\right]$	$\tilde{V}(\vec{p}) = -\frac{e^2}{\vec{p}^2}\left[1 + \frac{q_M^2 \vec{p}^2}{480\pi^2 m^2}\right]$
$V(r) = -\frac{e^2}{4\pi r}\left[1 - \frac{q_M^2 \pi}{3}(\gamma_e + \ln(mr))\right]$	$V(r) = -\frac{e^2}{4\pi r}\left[1 + \frac{q_M^2 r}{120\pi m^2}\delta^{(3)}(\vec{r})\right]$
$\Delta E = -\frac{e^2 q_M^2}{144 a_o}$	$\Delta E = -\frac{e^2}{3840\pi^3 a_o^3}\left(\frac{q_M}{m}\right)^2$

where a_o is the Bohr radius and r is the distance between the electron and proton.

Discussion

Before plotting the charge versus the mass, there are a two things to be addressed. Firstly, a quantitative criteria is required as to where the mass limits will fail. Since $a_o \sim \frac{1}{m_e} \implies p \sim \frac{1}{a_o}$, the mass limits become: $m^2 >> \frac{1}{a_o^2}$ and $m^2 << \frac{1}{a_o^2}$.

Secondly, to utilize the Lamb Shift, its value is necessary. From [19], the best experimental for the Lamb Shift is 1057.845(3)MHz. To analyze the effect the MCP would have on the Lamb Shift, we are interested in the measurement's error bound. Due to the fact the MCP effect must be smaller than the observed value, ΔE must be less than the experimental error bound so $\Delta E < 3$kHz.

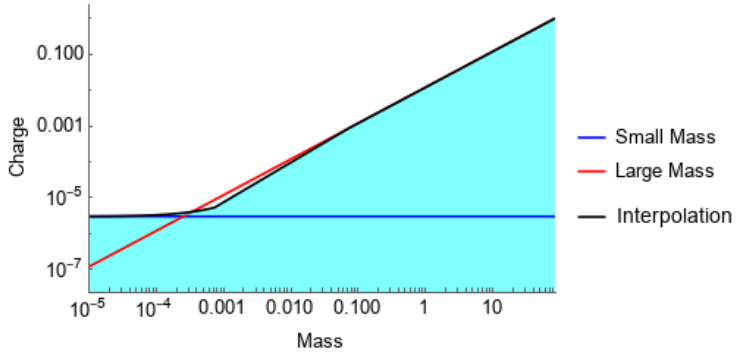

Figure 1: Log-log exclusion plot of charge as a function of mass. The cyan shading represents the region of possible values for q_M and m. Other than the limitations from the Lamb Shift, no other restrictions were included on the plot. The charge is with respect to e and mass with respect to m_e.

The mass range was plotted from $m = 0$ to the value of m corresponding to $\epsilon = 1$, which is $\mu = 84.275$. Of course, $\epsilon = 1$ is far too large, but it was picked as to not exclude any part of the phase space[1]. The curve could be plotted indefinitely, but, for $\mu > 84.275$, any points above $\epsilon = 1$ would not be shaded. However, as will be discussed below, anything further does not contribute any new information. In the plot, the space in between the mass limits was interpolated. With 10% error, we are assuming the limiting cases are accurate in $\mu \in \left(0, 7.297 \times 10^{-4}\right) \cup \left(7.297 \times 10^{-2}, \infty\right)$, while the interpolation serves as an acceptable approximation between the two limits. Though, no quantitative statement can be made from the interpolation.

As one can note, the plot correctly predicts the result if $\epsilon = 0$. MCP would not interact with matter, have no effect on the Lamb Shift, so we would get $\Delta E = 0$. In which case, searching for it via the Lamb Shift would be futile, so let us analyze what $\Delta E \neq 0$ yields. In Figure 1, $\epsilon > 0.001$ at $\mu = 1$ and increases linearly. The current limitations on ϵ (ranging from $10^{-5} - 0.1$) have been well surpassed. Therefore, it is evident our analysis contributes no further restriction, which is why a larger range of m was not covered in Figure 1.

For $\mu < 1$ but $\mu > 1.957 \times 10^{-3}$, it can be discerned that around $\mu = 0.002$, from the interpolation, $\epsilon < 3.4 \times 10^{-5}$. Since the interpolation is only an approximation, no conclusive cut off point can be made, except for there is some limit imposed in this region. For $\mu < 1.957 \times 10^{-3}$, it is evident, from the interpolation, $\epsilon < 1 \times 10^{-5}$; other than the fact ϵ can be further constrained at each value of $\mu \in \left(7.297 \times 10^{-4}, 1.957 \times 10^{-3}\right)$, nothing more can be concluded. However, we know, for $\mu \leq 7.297 \times 10^{-4}$ (with $\geq 90\%$ accuracy), q_M is dominated by the low mass limit. Therefore, it can be conclude $\epsilon < 3.011 \times 10^{-6}$.

[1] From the $\mu > 1.957 \times 10^3$ constraint, $\epsilon \leq 0.1 \, \forall \mu$. This was ignored in the shading as explained in Figure 1.

This lowers the current limitation in the region by $\approx \frac{1}{3}$.

For future, it would be essential to plot the full solution to ΔE- not just the mass limits and the interpolation- so that conclusive, quantitative results in the interpolation regions can be deduced. Albeit higher order corrections (beyond 1-loop) to the Coulomb potential would have a minor effect on the overall result, it would still be of benefit to examine what effects they would have on q_M and m.

Conclusion

The objective of this paper was to determine the constraints on the scalar MCP's charge-mass phase space. This was accomplished by considering the contribution of the 1-loop corrections to the Coulomb potential due to MCP, thereby allowing for the effect on the Lamb Shift to be calculated. From this, a charge-mass exclusion plot determined what values of q_M and m are possible according to the Lamb Shift. Albeit no new restriction were placed on q_M for $\mu > 1$, the current limit of $\epsilon < 1 \times 10^{-5}$ for $\mu \leq 7.297 \times 10^{-4}$ was constrained to $\epsilon < 3.011 \times 10^{-6}$.

For future, as discussed, the full solution to ΔE must be plotted so that quantitative results in the interpolation region can be deduced since it is evident there will be some restriction on the currents limits. As well, higher order corrections to the Coulomb potential can always be computed to observe the minor effects they will have on q_M and m.

Appendices

Appendix A: Feynman Rules

Here are the Feynman Rules [13] we utilized:

- MCP propagator: $\tilde{\Delta}(p) = \frac{i}{p^2 - m^2 + i\epsilon'}$
- MCP two vertices:
    1. Figure 2 to 5 has a vertex factor of: $-iq_M \left[\alpha_1 p_1^\mu + \alpha_2 p_2^\nu\right]$, where $\alpha_j = 1$ for MCP and $\alpha_j = -1$ for anti-MCP for $j \in [1, 2]$, the particle on the left (for a vertex with only MCP or anti-MCP) gets labeled with p_1^μ, and- for a vertex with a MCP and anti-MCP- the MCP gets labeled with p_1^μ.
    2. Figure 6 has a vertex factor of: $2iq_M^2 g^{\mu\nu}$
- Photon propagator: $D^o_{\mu\nu} = \frac{-ig_{\mu\nu}}{p^2 + i\epsilon'}$
- Incoming and outgoing fermion external line's spinors are: $u^{(s)}(p)$ and $\bar{u}^{(s)}(p)$, respectively.
- Incoming and outgoing anti-fermion external line's spinors are: $\bar{v}^{(s)}(p)$ and $v^{(s)}(p)$, respectively.
- Fermion vertex: $-iq_f\gamma^\mu$.

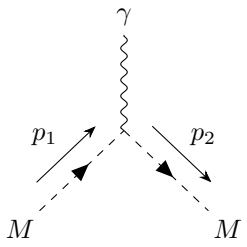

Figure 2: MCP Scattering Vertex

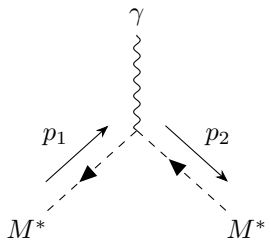

Figure 3: Anti-MCP Scattering Vertex

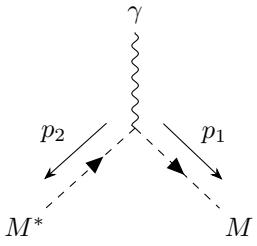

Figure 4: MCP and Anti-MCP Creation Vertex

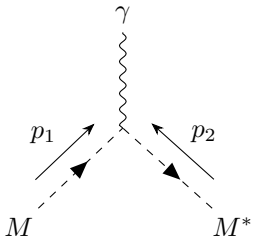

Figure 5: MCP and Anti-MCP Annihilation Vertex

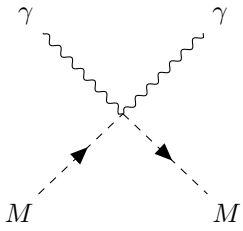

Figure 6: Four Particle Vertex for MCP

Appendix B: Identities

Here are identities that are used. Identity 1 to 2 are from [13]. Below, identity 4 will be derived.

1. $\int \frac{1}{(k^2-\Delta+i\epsilon')} \frac{d^D k}{(2\pi)^D} = \frac{i}{(4\pi)^{\frac{D}{2}}} \frac{1}{\Delta^{2-\frac{D}{2}}} \Gamma\left(2-\frac{D}{2}\right)$
2. $\int \frac{k^2}{(k^2-\Delta+i\epsilon')} \frac{d^D k}{(2\pi)^D} = \frac{-D}{2} \frac{i}{(4\pi)^{\frac{D}{2}}} \frac{1}{\Delta^{1-\frac{D}{2}}} \Gamma\left(1-\frac{D}{2}\right)$
3. Taylor Expansion about $\epsilon' = 0$: $x^{a\epsilon'} = 1 + a\ln(x)\epsilon' + \mathcal{O}(\epsilon^2)$
4. Taylor Expansion about $\epsilon' = 0$: $\Gamma\left(\frac{\epsilon'}{2}\right) = \frac{2}{\epsilon'} - \gamma_e + \frac{\epsilon'}{4}\left(\gamma_e^2 + \frac{\pi^2}{6}\right) + \mathcal{O}(\epsilon'^2)$

Here is the derivation of identity 4. In its evaluation, we will use integration by parts, the fact $t^{\frac{\epsilon'}{2}} = \sum_{n=0}^{\infty} \left(\frac{\epsilon'}{2}\right)^n \frac{\ln^n(t)}{n!}$, and Mathematica to evaluate the integrals.

$$\Gamma\left(\frac{\epsilon'}{2}\right) = \int_0^\infty e^{-t} t^{\frac{\epsilon}{2}-1} dt = \frac{2}{\epsilon'} \int_0^\infty e^{-t} t^{\frac{\epsilon'}{2}} dt$$

$$= \sum_{n=0}^{\infty} \left(\frac{\epsilon'}{2}\right)^{n-1} \frac{1}{n!} \int_0^{\infty} e^{-t} \ln^n(t) dt$$
$$= \frac{2}{\epsilon'} - \gamma_e + \frac{\epsilon'}{4}\left(\gamma_e^2 + \frac{\pi^2}{6}\right) + \mathcal{O}(\epsilon'^2)$$

Appendix C: Corrected Coulomb Potential Calculation

Evaluating the Feynman Diagrams

$$\begin{aligned} i\Pi_2^{\mu\nu} &= q_M^2 \int \frac{(2q^\mu - p^\mu)(2q^\nu - p^\nu) - 2g^{\mu\nu}\left((q-p)^2 - m^2\right)}{((q-p)^2 - m^2 + i\epsilon')\left(q^2 - m^2 + i\epsilon'\right)} \frac{d^4q}{(2\pi)^4} \\ &= q_M^2 \int \frac{4q^\mu q^\nu - 2q^\mu p^\nu - 2p^\mu q^\nu + p^\mu p^\nu - 2g^{\mu\nu}\left((q-p)^2 - m^2\right)}{((q-p)^2 - m^2 + i\epsilon')\left(q^2 - m^2 + i\epsilon'\right)} \frac{d^4q}{(2\pi)^4} \\ &= q_M^2 \int \frac{4q^\mu q^\nu - 2q^\mu p^\nu - 2p^\mu q^\nu - 2g^{\mu\nu}\left((q-p)^2 - m^2\right)}{((q-p)^2 - m^2 + i\epsilon')\left(q^2 - m^2 + i\epsilon'\right)} \frac{d^4q}{(2\pi)^4} \end{aligned}$$

where $p^\mu p^\nu$ can be ignored due to gauge invariance (i.e. the Ward Identity); this fact will be used throughout the derivation. Feynman Parameters will be introduced- namely, $\frac{1}{AB} = \int_0^1 \frac{1}{[A+(B-A)x]^2} dx$. Calculating the $[A + (B-A)x]$ term:

$$\begin{aligned} &\left((q-p)^2 - m^2 + i\epsilon'\right)\left(q^2 - m^2 + i\epsilon'\right) \\ =&(q-p)^2 - m^2 + i\epsilon' + \left[q^2 - (q-p)^2\right] x \\ =&(q - p(1-x))^2 - p^2x(1-x) - m^2 + i\epsilon' \end{aligned}$$

Let $\lambda^\mu = q^\mu - p^\mu(1-x)$:

$$\begin{aligned} i\Pi_2^{\mu\nu} &= q_M^2 \int_0^1 \int \frac{4q^\mu q^\nu - 2q^\mu p^\nu - 2p^\mu q^\nu - 2g^{\mu\nu}\left((q-p)^2 - m^2\right)}{\left[(q-p(1-x))^2 - p^2x(1-x) - m^2 + i\epsilon'\right]^2} dx \frac{d^4q}{(2\pi)^4} \\ &= 2q_M^2 \int_0^1 \int \frac{2\lambda^\mu\lambda^\nu + \lambda^\mu p^\nu(1-2x) + p^\mu\lambda^\nu(1-2x) - g^{\mu\nu}\left((\lambda - px)^2 - m^2\right)}{\left[\lambda^2 - p^2x(1-x) - m^2 + i\epsilon'\right]^2} dx \frac{d^4\lambda}{(2\pi)^4} \\ &= 2q_M^2 \int_0^1 \int \frac{2\lambda^\mu\lambda^\nu - g^{\mu\nu}\left(\lambda^2 + p^2x^2 - m^2\right)}{\left[\lambda^2 - p^2x(1-x) - m^2 + i\epsilon'\right]^2} dx \frac{d^4\lambda}{(2\pi)^4} \end{aligned}$$

where we used the fact $2g^{\mu\nu}\lambda px$, $\lambda^\mu p^\nu(1-2x)$, and $p^\mu\lambda^\nu(1-2x)$ are odd under $d^4\lambda$.

At this point, a regularization method will need to be utilized; we will use Dimensional Regularization. Since all physical quantities are finite, yet our integrals are divergent, it is a method to regulate the integrals by isolating the divergence, which will allow us to calculate the integral and remove the divergence through renormalization. A regulator, ϵ', will be introduced to isolate the divergence; this will yield a finite result,

except when $\epsilon' \mapsto 0$. For Dimensional Regularization, the dimension of space-time is extended to D-dimensional space; in the end, D will be set equal to $D = 4 - \epsilon'$. As we let $\epsilon' \mapsto 0$ and expand terms about $\epsilon' = 0$, our divergence will become a pole. To ensure $\Pi_2^{\mu\nu}$ is dimensionless, a mass scale, $\mu^{2-\frac{D}{2}}$, will be introduced. Introducing the regulator, using the fact $\lambda^\mu \lambda^\nu \to \frac{1}{D}\lambda^2 g^{\mu\nu}$, and introducing the mass scale by $q_M \to q_M \mu^{2-\frac{D}{2}}$, one obtains:

$$
\begin{aligned}
i\Pi_2^{\mu\nu} &= 2q_M^2 \mu^{4-D} \int_0^1 \int \frac{\frac{2}{D}\lambda^2 g^{\mu\nu} - g^{\mu\nu}\left(\lambda^2 + p^2x^2 - m^2\right)}{\left[\lambda^2 - p^2x(1-x) - m^2 + i\epsilon'\right]^2} dx \frac{d^D\lambda}{(2\pi)^D} \\
&= 2q_M^2 \mu^{4-D} g^{\mu\nu} \int_0^1 \int \frac{\left(\frac{2}{D} - 1\right)\lambda^2 - \left(p^2x^2 - m^2\right)}{\left[\lambda^2 - p^2x(1-x) - m^2 + i\epsilon'\right]^2} dx \frac{d^D\lambda}{(2\pi)^D} \\
&= \frac{-2iq_M^2 g^{\mu\nu}}{(4\pi)^{\frac{D}{2}}} \mu^{4-D} \int_0^1 \left[\frac{1 - \frac{D}{2}}{\left(p^2x(x-1) + m^2\right)^{1-\frac{D}{2}}} \Gamma\left(1 - \frac{D}{2}\right)\right] - \left[\frac{p^2x^2 - m^2}{\left(p^2x(x-1) + m^2\right)^{2-\frac{D}{2}}} \Gamma\left(2 - \frac{D}{2}\right)\right] dx \\
&= \frac{-2ip^2q_M^2 g^{\mu\nu}}{(4\pi)^{\frac{D}{2}}} \mu^{4-D} \Gamma\left(2 - \frac{D}{2}\right) \int_0^1 \frac{x(2x-1)}{\left(p^2x(x-1) + m^2\right)^{2-\frac{D}{2}}} dx
\end{aligned}
$$

where identity 1 and 2 (from Appendix B) were used. Expanding the terms about $\epsilon' = 0$ and using identity 3 and 4 (from Appendix B):

$$
\begin{aligned}
i\Pi_2^{\mu\nu} &= \frac{-2ip^2q_M^2 g^{\mu\nu}}{(4\pi)^{2-\frac{\epsilon'}{2}}} \mu^{\epsilon'} \Gamma\left(\frac{\epsilon'}{2}\right) \int_0^1 \frac{x(2x-1)}{\left(p^2x(x-1) + m^2\right)^{\frac{\epsilon'}{2}}} dx \\
&= \frac{-ip^2q_M^2 g^{\mu\nu}}{8\pi^2} \int_0^1 \left[\frac{2}{\epsilon'} - \gamma_e + 2\ln(\mu) + \ln(4\pi) - \ln(p^2x(x-1) + m^2) + \mathcal{O}(\epsilon')\right] x(2x-1) dx \\
&= \frac{-ip^2q_M^2 g^{\mu\nu}}{8\pi^2} \int_0^1 x(2x-1)\left[\frac{2}{\epsilon'} + \ln\left(\frac{4\pi e^{-\gamma_e}\mu^2}{p^2x(x-1) + m^2}\right) + \mathcal{O}(\epsilon')\right] dx \\
&= -iq_M^2 p^2 g^{\mu\nu} \Pi_2(p)
\end{aligned}
$$

Born Approximation

We are looking at an electron-proton scattering in the non-relativistic limit. To establish a relationship between the Coulomb potential and the scattering amplitude, we will use the Born Approximation and the differential cross section of the scattering, which are $\frac{d\sigma}{d\Omega} = \frac{m_e^2}{4\pi^2}\left[\tilde{V}(p)\right]^2$ and $\frac{d\sigma}{d\Omega} = \frac{1}{64\pi^2 m_p^2}\left[\mathcal{M}\right]^2$, respectively [13], where m_e and m_p are the electron and proton's mass, respectively. For the differential cross section, the center of mass frame is approximated as the proton's rest frame, and the process is assumed to be elastic scattering.

The electron-proton t-channel diagram, where $D_{\mu\nu}$ replaces $D^o_{\mu\nu}$, will give us the matrix element. In the non-relativistic limit, we are left with D_{00} [22], which yields:

$$
\begin{aligned}
i\mathcal{M} &= \bar{u}^3(p_3)(-iq_f\gamma^\mu)u^1(p_1)D_{\mu\nu}\bar{u}^4(p_4)(-iq_f\gamma^\nu)u^2(p_2) \\
&= 4iq_f^2 m_e m_p \frac{1}{p^2}\left[1 - q_M^2\Pi_2(p)\right] \\
\therefore |\mathcal{M}| &= 4q_f^2 m_e m_p \frac{1}{p^2}\left[1 - q_M^2\Pi_2(p)\right]
\end{aligned}
$$

Relating the two differential cross sections:

$$
\begin{aligned}
&\frac{d\sigma}{d\Omega} = \frac{m_e^2}{4\pi^2}\left[\tilde{V}(p)\right]^2 = \frac{1}{64\pi^2 m_p^2}\left[\mathcal{M}\right]^2 \\
&\implies \frac{m_e}{2\pi}\tilde{V}(p) = \frac{1}{8\pi m_p}|\mathcal{M}| \\
&\implies \tilde{V}(p) = \frac{q_f^2}{p^2}\left[1 - q_M^2\Pi_2(p)\right]
\end{aligned}
$$

Appendix D: Mass Limits

For Electrostatics, the static case of the momentum will be considered. Let $p^2 = -\vec{p}^2$, then $\tilde{V}(p) = \frac{e^2}{p^2}\left[1 - q_M^2\Pi_2^R(p)\right] \mapsto \tilde{V}(\vec{p}) = -\frac{e^2}{\vec{p}^2}\left[1 - q_M^2\Pi_2^R(\vec{p})\right]$, where $\Pi_2^R(\vec{p}) = \frac{1}{8\pi^2}\int_0^1 x(2x-1)\ln\left(\frac{m^2}{\vec{p}^2x(1-x)+m^2}\right)dx$. The two mass limits will be examined. Mathematica will evaluate all the integrals. For the $m^2 << \vec{p}^2$ case:

$$
\begin{aligned}
\Pi_2^R(\vec{p}) =& \frac{1}{8\pi^2}\int_0^1 x(2x-1)\ln\left(\frac{m^2}{\vec{p}^2x(1-x)+m^2}\right)dx \\
\approx& -\frac{1}{8\pi^2}\int_0^1 x(2x-1)\ln\left(\frac{\vec{p}^2}{m^2}x(1-x)\right)dx \\
\approx& -\frac{1}{48\pi^2}\ln\left(\frac{\vec{p}^2}{m^2}\right)
\end{aligned}
$$

The Fourier transform of $\tilde{V}(\vec{p})$ can now be found. We will examine the second term in $\tilde{V}(\vec{p})$ since the first term will, obviously, gives us $-\frac{e^2}{4\pi r}$.

$$
\begin{aligned}
\tilde{V}_{term_2}(\vec{p}) &= -\frac{e^2q_M^2}{48\pi^2\vec{p}^2}\ln\left(\frac{\vec{p}^2}{m^2}\right) \\
V_{term2}(r) &= -\frac{e^2q_M^2}{48\pi^2}\int\frac{\ln\left(\frac{\vec{p}^2}{m^2}\right)}{\vec{p}^2}e^{-i\vec{p}\cdot\vec{r}}d^3p \\
&= -\frac{e^2q_M^2}{48\pi^2}\int_0^\infty\int_0^\pi\int_0^{2\pi}\frac{\ln\left(\frac{\rho^2}{m^2}\right)}{\rho^2}\rho^2 sin(\theta)e^{-i\rho r\cos(\theta)}d\rho d\theta d\phi \\
&= -\frac{e^2q_M^2}{12\pi r}\int_0^\infty\frac{\ln\left(\frac{\rho^2}{m^2}\right)}{\rho}\sin(\rho r)d\rho
\end{aligned}
$$

$$= \frac{e^2 q_M^2}{12r} \left[\gamma_e + \ln(mr)\right]$$
$$\therefore V(r) = -\frac{e^2}{4\pi r} + \frac{e^2 q_M^2}{12r} \left[\gamma_e + \ln(mr)\right]$$

For the $m^2 >> \vec{p}^2$ case:

$$\begin{aligned}
\Pi_2^R(\vec{p}) =& \frac{1}{8\pi^2} \int_0^1 x(2x-1) \ln\left(\frac{m^2}{\vec{p}^2 x(1-x) + m^2}\right) dx \\
=& -\frac{1}{8\pi^2} \int_0^1 x(2x-1) \ln\left(1 + \frac{\vec{p}^2}{m^2} x(1-x)\right) dx \\
\approx& -\frac{1}{8\pi^2} \int_0^1 x(2x-1) \frac{\vec{p}^2}{m^2} x(1-x) dx \\
=& -\frac{1}{480\pi^2} \frac{\vec{p}^2}{m^2}
\end{aligned}$$

The Fourier transform of $\tilde{V}(\vec{p})$ can now be found:

$$\tilde{V}(\vec{p}) = -\frac{e^2}{\vec{p}^2} \left[1 + \frac{q_M^2 \vec{p}^2}{480\pi^2 m^2}\right]$$
$$V(r) = -\frac{e^2}{4\pi r} - \frac{e^2 q_M^2}{480\pi^2 m^2} \delta^3(\vec{r})$$

where the Fourier transform will be stated without proof (it is readily found since it is identical, apart from constants, to the one from Quantum Electrodynamics [13, 22]).

Appendix E: Determining ΔE

For the Lamb Shift, $\Delta E = \Delta E(2S_{\frac{1}{2}}) - \Delta E(2P_{\frac{1}{2}})$. Mathematica will evaluate all the integrals. For the $m^2 << \vec{p}^2$ case, $\Delta V(r) = \frac{e^2 q_M^2}{12r} \left[\gamma_e + \ln(mr)\right]$. Since $\psi_{200}(r) = \frac{1}{4\sqrt{2\pi a_o^3}} \left[2 - \frac{r}{a_o}\right] e^{-\frac{r}{2a_o}}$ [10]:

$$\begin{aligned}
\Delta E(2S_{\frac{1}{2}}) &= \langle \psi_{200}(r) | \Delta V(r) | \psi_{200}(r) \rangle \\
&= \frac{e^2 q_M^2}{12} \left[\gamma_e \langle \psi_{200}(r) | \left(\frac{1}{r}\right) | \psi_{200}(r) \rangle + \langle \psi_{200}(r) | \left(\frac{\ln(mr)}{r}\right) | \psi_{200}(r) \rangle\right] \\
&= \frac{e^2 q_M^2}{48 a_o} \left[\ln(a_o m) + \frac{3}{2}\right]
\end{aligned}$$

Since $\psi_{210} = \frac{1}{4\sqrt{2\pi a_o^5}} r \cos(\theta) e^{-\frac{r}{2a_o}}$ [10]:

$$\Delta E(2P_{\frac{1}{2}}) = \langle \psi_{210}(r) | \Delta V(r) | \psi_{210}(r) \rangle$$

$$= \frac{e^2 q_M^2}{12}\left[\gamma_e \langle\psi_{210}(r)|\left(\frac{1}{r}\right)|\psi_{210}(r)\rangle + \langle\psi_{210}(r)|\left(\frac{\ln(mr)}{r}\right)|\psi_{210}(r)\rangle\right]$$
$$= \frac{e^2 q_M^2}{48 a_o}\left[\ln(a_o m) + \frac{11}{6}\right]$$

Subtracting the two results:

$$\Delta E = -\frac{e^2 q_M^2}{144 a_o}$$

For the $m^2 >> \vec{p}^2$ case, $\Delta V(r) = -\frac{e^2 q_M^2}{480\pi^2 m^2}\delta^3(\vec{r})$. It is obvious $\Delta E(2P_{\frac{1}{2}}) = 0$ due to the fact, at $r = 0$, only $l = 0$ levels are non-zero. Therefore, we find ΔE is:

$$\begin{aligned}\Delta E &= \langle\psi_{200}(r)|\Delta V(r)|\psi_{200}(r)\rangle \\ &= -\frac{e^2 q_M^2}{480\pi^2 m^2}|\psi_{200}(0)|^2 \\ &= -\frac{e^2 q_M^2}{3840\pi^3 a_o^3 m^2}\end{aligned}$$

References

[1] A.A. Prinz, *et al.* "Search for Millicharged Particles at SLAC." Phys. Rev. Lett. **81** (6), p.g. 1175-1178 (1998). doi:10.1103/physrevlett.81.1175.

[2] A. Badertcher, *et al.* "Improved limit on invisible decays of positronium." Phys. Rev. D **75** (3) (2007). doi:10.1103/physrevd.75.032004.

[3] A.D. Dolgov, *et al.* "Constraints on millicharged particles from Planck data." Phys. Rev. D **88** (11) (2013). doi:10.1103/physrevd.88.117701.

[4] A.Y. Ignatiev, V.A. Kuzmin, and M.E. Shaposhnikov. "Is the electric charge conserved?" Phys. Lett. B **84** (3), p.g. 315-318 (1979). doi:10.1016/0370-2693(79)90048-0.

[5] B. Batell, M. Pospelov, and A. Ritz. "Exploring portals to a hidden sector through fixed targets." Phys. Rev. D **80** (9) (2009). doi:10.1103/physrevd.80.095024.

[6] B. Döbrich, *et al.* "Magnetically amplified light-shining-through-walls via virtual minicharged particles." Phys. Rev. D **87** (2) (2013). doi:10.1103/physrevd.87.025022.

[7] B. Döbrich, *et al.* "Magnetically Amplified Tunneling of the Third Kind as a Probe of Minicharged Particles." Phys. Rev. Lett. **109** (13) (2012). doi:10.1103/physrevlett.109.131802.

[8] B. Holdom. "Two $U(1)$'s and ϵ charge shifts." Phys. Lett. B **166** (2), p.g. 196-198 (1986). doi:10.1016/0370-2693(86)91377-8.

[9] C. Burrage, *et al.* "Late time CMB anisotropies constrain mini-charged particles." J. of Cosmology and Astroparticle Phys. **2009** (11), p.g. 002-002 (2009). doi:10.1088/1475-7516/2009/11/002.

[10] D.J. Griffiths. *Introduction to Quantum Mechanics*. Cambridge University Press, 2017.

[11] E. Izaguirre and I. Yavin. "New window to millicharged particles at the LHC." Phys. Rev. D **92** (3) (2015). doi:10.1103/physrevd.92.035014.

[12] G. Magill, *et al.* "Millicharged Particles in Neutrino Experiments." Phys. Rev. D **122** (7) (2019). doi:10.1103/physrevd.122.071801.

[13] M. D. Schwartz. *Quantum Field Theory and the Standard Model*. Cambridge University Press, 2014.

[14] J.J. Krauth, *et al.* "Paving the way for fundamental physics tests with singly-ionized helium." arXiv:1910.13192 [atom-ph] (2019).

[15] K.J. Kelly and Y. Tsai. "Proton fixed-target scintillation experiment to search for millicharged dark matter." Phys. Rev. D **100** (1) (2019). doi:10.1103/physrevd.100.015043.

[16] L. Singh, *et al.* "Constraints on millicharged particles with low-threshold germanium detectors at Kuo-Sheng Reactor Neutrino Laboratory." Phys. Rev. D **99** (3) (2019). doi:10.1103/physrevd.99.032009.

[17] M. Ahlers. "The Hubble diagram as a probe of minicharged particles." Phys. Rev. D **80** (2) (2009). doi:10.1103/physrevd.80.023513.

[18] R. Harnik, Z. Liu, and O. Palamara. "Millicharged particles in liquid argon neutrino experiments." J. of High Energy Phys. **2019** (7) (2019). doi:10.1007/jhep07(2019)170.

[19] M.I. Eides, H. Grotch, and V.A. Shelyuto. "Theory of light hydrogenlike atoms." Phys. Reports **342** (2-3), p.g. 63-261 (2001). doi:10.1016/s0370-1573(00)00077-6.

[20] R. Escribano and E. Masso. "High precision tests of QED and physics beyond the standard model." The European Physical J. C. **4** (1), p.g. 139-143 (1998). doi:10.1007/pl00021656.

[21] R. Szafron, *et al.* "Virtual Delbrück scattering and the Lamb Shift in light hydrogenlike atoms." Phys. Rev. A **100** (3) (2019). doi:10.1103/physreva.100.032507.

[22] S.J. Blundell and T. Lancaster. *Quantum Field Theory for the Gifted Amateur*. Oxford University Press, 2014.

[23] S.N. Gninenko, D.V. Kirpichnikov, and N.V. Krasnikov. "Probing millicharged particles with NA64 experiment at CERN." Phys. Rev. D **100** (3) (2019). doi:10.1103/physrevd.100.035003.

[24] X. Huang, *et al.* "Constraints on millicharged particles by neutron stars." Phys. Rev. D **91** (12) (2015). doi:10.1103/physrevd.91.123513.

[25] Z. Berezhiani, A. Dolgov, and I. Tkachev. "BBN with light dark matter." J. of Cosmology and Astroparticle Phys. **2013** (02), p.g. 010-010 (2013). doi:10.1088/1475-7516/2013/02/010.